Development of a Lightweight Underwater Manipulator for Delicate Structural Repair Operations

Juzheng Mao[1], Guangming Song[1], Senior Member, IEEE, Shuang Hao[1], Mingquan Zhang[1], and Aiguo Song[1], Senior Member, IEEE

***Abstract*—In recent years, underwater robots have been increasingly used in the maintenance of hydraulic structures. Underwater manipulators are essential devices that are used to carry out such maintenance tasks. For delicate repair operations such as fixing tiny cracks, most existing underwater manipulators face limitations in terms of size, accuracy, and scalability. Therefore, in this letter, we present a novel electric underwater manipulator, named SEU-4. This four-degree-of-freedom manipulator weighs 8.91 kg and has a maximum payload of 9 kg. It has a rapid-switching interface that supports convenient mechanical and electrical connections for end-effectors. To compensate for the disturbances that are present in the complex underwater environment, a trajectory-tracking control strategy based on a disturbance observer and sliding-mode control (DOB-SMC) is proposed. A prototype of the proposed underwater manipulator was created, and a flowing-water experimental platform was constructed to test its trajectory-tracking performance in fast-flowing water. The experimental results show that the manipulator achieves a trajectory-tracking error of 1.03 mm in static water and 2.91 mm in flowing water at 1.2 m/s, which satisfies the requirements of delicate repair operations.**

I. Introduction

Carrying out maintenance work on hydraulic structures is challenging because most of the underwater manipulations involved currently have to be done manually. In recent years, advances in technology have enabled increasing use of underwater robots in infrastructure-maintenance tasks; underwater manipulators are essential components for carrying out such tasks. These manipulators can be generally classified into two types: hydraulically driven and electrically driven. Hydraulic manipulators generally have high force/torque outputs, but this comes with the drawbacks of low position accuracy and unavoidable leakage of hydraulic oil [1]. Hydraulic manipulators are suitable for most industrial tasks that require high speed, strength, or force [2], but they are not suitable for use in tasks involving delicate repair operations. Electrically actuated manipulators offer the advantages of precise motion and force/torque control [3]; however, the technology of existing electric underwater manipulators is not yet mature, and it has limitations in load-to-weight ratios and scalability. Thus, this letter concerns the development of a novel electric underwater manipulator.

Underwater manipulators are typically mounted on uncrewed underwater vehicles (UUVs). As such, the weight and size of a manipulator are very important factors that directly impact the amount of dynamic coupling between it and the underwater robot to which it is attached [4]. Reducing the weight of a manipulator can effectively reduce its coupling with a UUV, and this will improve operational accuracy.

There are currently some lightweight manipulators that are commercially available, and these include both electric and hydraulic types, as shown in Table I. The lightest commercially available hydraulic manipulator weighs 6 kg [4], while the lightest electric manipulator weighs 9 kg [5]. These manipulators have been used in various operations such as underwater surface cleaning, mine disposal, archaeological work, salvage of sunken objects, geological sampling, cable laying and maintenance, underwater pipe inspection, switching valves, drilling, rope cutting, and grasping marine organisms [6]–[13].

Research groups worldwide have also developed some lightweight electric underwater manipulators for research purposes. For instance, Skaldebø *et al.* [1] developed SeaArm-2, a lightweight manipulator weighing 3.58 kg with a gripper integrated as the end-effector; they conducted grasping experiments in a static water environment. Wang *et al.* [14] developed a novel manipulator mainly for grasping; tests of this manipulator were conducted in a static water tank. Shen *et al.* [15] proposed an underwater hybrid manipulator with a lightweight actuation control system primarily intended for grasping. Additionally, Gong *et al.* [16] designed a soft pneumatic manipulator capable of delicately grasping seafood animals, and this had a location error of 13.4 mm. Koch *et al.* [17] developed a manipulator named AquaSimian; this was tested for valve-turning in real marine environments at a water-flow velocity of close to zero.

Most of the underwater manipulators mentioned above are integrated with grippers for grasping operations only, and they are not suitable for carrying different tools as end-effectors. They therefore face significant challenges when it comes to delicate repair operations such as fixing tiny cracks in underwater structures. These tiny cracks are typically in the millimeter range; the process of repairing them is complex, and it requires multiple tools. To complete a repair, an ideal underwater manipulator must be lightweight, possess sufficient payload capacity, exhibit high trajectory accuracy, and have the ability to use multiple end-effectors to adapt to different

Manuscript received: May 30, 2023; Revised: August 11, 2023; Accepted: August 16, 2023. This paper was recommended for publication by Editor Hyungpil Moon upon evaluation of the Associate Editor and Reviewers' comments. This work was supported in part by the National Natural Science Foundation of China under Grant 61973076 and Grant 52127813 and the National Key Research and Development Program of China (No.2020YFC1511904). (Corresponding author: Guangming Song.)

[1] Juzheng Mao, Guangming Song, Shuang Hao, Mingquan Zhang and Aiguo Song are with the State Key Laboratory of Digital Medical Engineering, Jiangsu Key Lab of Remote Measurement and Control, School of Instrument Science and Engineering, Southeast University, Nanjing 210096, China (e-mail: j.mao@ieee.org; mikesong@seu.edu.cn; haoshuang23@163.com; mingquan_zhang@seu.edu.cn; a.g.song@seu.edu.cn).

Digital Object Identifier (DOI): see top of this page.

IEEE Robotics and Automation Letters (RA-L) paper, presented at ICRA 2024, Yokohama, Japan. Cite as RA-L paper.

TABLE I
SPECIFICATIONS OF TYPICAL EXISTING COMMERCIAL UNDERWATER MANIPULATORS AND RESEARCH PROTOTYPES.

Developer	Model	Actuation	DoF	Reach (m)	Weight (kg)	Payload (kg)	Error (mm)	Material
Hydro-Lek	43000	Hydraulic	4	0.53	6	10	-	Stainless Steel (SS)
TitanRob	M501	Hydraulic	4	0.95	14	40	-	Titanium Alloy, SS
Graal Tech	UMA	Electric	6	1	28	10	0.5	Aluminium Alloy (AL)
ECA Group	ARM 5E Micro	Electric	4	0.6	10	10	-	AL
HDT Global	HDT-MK3-M	Electric	6	0.8	9	-	40	AL
Justin *et al.*	AquaSimian	Electric	6	1.25	50	5	-	AL
Wang *et al.*	-	Electric	4	0.6	11.9	-	-	AL
Skaldebø *et al.*	SeaArm-2	Electric	4	0.7	3.58	5	-	AL
Gong *et al.*	-	Pneumatic	3	0.6	1.05	-	13.4	Silica Gel
Our Group	**SEU-4**	**Electric**	**4**	**0.6**	**8.91**	**9**	**1.03**	**AL**

phases of a repair operation. The manipulator in [4] does not have joint angle sensors so it cannot perform closed-loop control. The end accuracy of [5] and [16] does not meet the 1mm requirement. The mass of the M501 and UMA manipulators in Table I is too large. Therefore, to the best of our knowledge, there are currently few lightweight manipulators that are suitable for such delicate maintenance operations.

Additionally, the underwater environment is complex and full of various disturbances, such as water flow and turbulence. These disturbances have a negative impact on the control of underwater manipulators. Researchers have proposed various control methods to achieve precise control of underwater manipulators [18]. Smith *et al.* were the first to apply proportional–integral–derivative (PID) controllers to underwater manipulators [19]. However, with PID control, it is difficult to eliminate control errors caused by external disturbances. Therefore, researchers began to study the nonlinear control of underwater manipulators. Oliveira *et al.* proposed an improved sliding-mode control (SMC) scheme, which was verified by simulations to improve the control accuracy of underwater manipulators [20]. Lee *et al.* proposed a control method that combines SMC with multi-layer neural networks to improve the real-time control performance of control models [21]. Most of the algorithms mentioned above have been validated only by simulations or in a static water environment, and they have not been tested in fast-flowing water.

Currently, SMC algorithms form the basis of most research examining motion-control methods for underwater manipulators. This approach can also be combined with other advanced control methods to improve the interference resistance and control accuracy of underwater manipulators. In this letter, a disturbance-observer-based SMC method (DOB-SMC) is proposed for underwater manipulator control. The DOB can be used as a feed-forward controller to adaptively resist disturbance according to the disturbance. This can calculate the interference of flowing water in real time and eliminate the high-frequency vibration effect caused by SMC.

The main contributions of this work are as follows.

1) A novel lightweight underwater manipulator was developed that is suitable for delicate underwater repairs.
2) A robust DOB-SMC controller is proposed and was deployed to improve the trajectory-tracking accuracy of the manipulator in fast-flowing water.
3) A rapidly deployable and cost-effective flowing-water test platform was constructed to verify the performance of this manipulator.

II. DESIGN CONCEPT AND KINEMATICS ANALYSIS

To meet the requirements outlined above, the design of the underwater manipulator should prioritize three things: low weight and small size to reduce coupling to the parent vehicle, high precision and load capacity to perform delicate operations with bulky end-effectors, and a rapid-switching end-effector interface to adapt to various tasks.

A. Lightweight Design

The lightweight design concept includes two aspects: first, the weight of the underwater manipulator needs to be minimized, and second, the manipulator should have a small footprint. As a result of adhering to these considerations, the final weight of the manipulator as designed is 8.91 kg, and it occupies only 0.02 m^3 of space. It is lighter than all of the commercial electric manipulators listed in Table I.

Aluminum alloy, stainless steel, and titanium alloy are materials that are commonly used in the manufacture of underwater manipulators. Aluminum alloy has the lowest density of these, which aids with the production of a lightweight design. The design of the structure of the underwater manipulator presented in this letter is shown in Fig. 1(a). The concept of integrated design was used to minimize the number of structural components as far as possible. The main structure was designed with only seven parts, as shown in Fig. 1(b), which lists all seven parts and their weights. The low total number of parts means that there are fewer assembly steps for the whole manipulator, therefore reducing the possibility of assembly errors. At the same time, reducing the number of connections reduces the probability of leakage. The complete manipulator has five static sealing parts and four dynamic

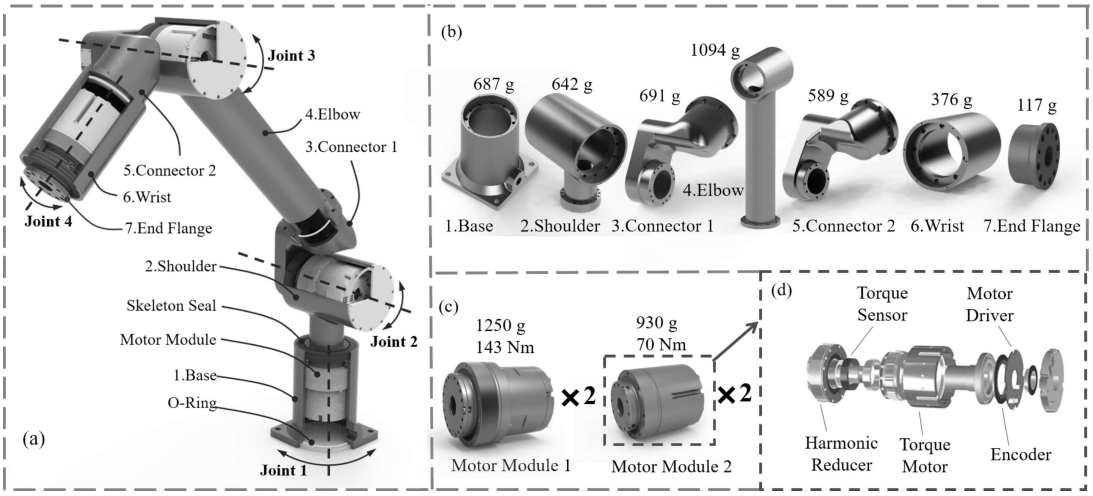

Fig. 1. Structure of the underwater manipulator: (a) overall view; (b) its seven structural parts and their weights; (c) the two types of motor module; (d) inner structure of the integrated motor module.

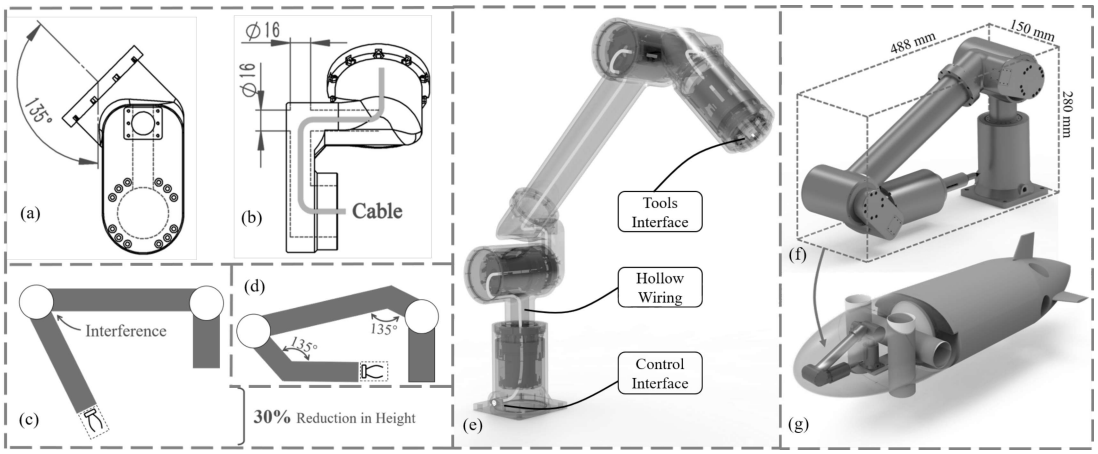

Fig. 2. Principle of low-footprint design. (a) 135° design of the connector makes the manipulator foldable. (b) The hollow design of the connector incorporates a 16-mm-diameter channel that can be used for wiring. (c) Interference of a straight-link manipulator. (d) Schematic diagram of the foldable design. (e) Wiring of the manipulator in the hollow internal space, including electrical interfaces. (f) Folded view of the manipulator with a marking tool as the end-effector. The occupied volume is indicated as a green wire frame. (g) Installation of the manipulator on a UUV in a confined space.

sealing parts. The static seals use O-rings, while the dynamic seals use double-layer skeleton seals. The installation locations of the seals are indicated in Fig. 1(a). With this seal design, it passed the test at the water pressure of 200 m. Theoretically, it can reach an ultimate depth of 300 m [22]. Two types of customized motor module are used in the manipulator, as shown in Fig. 1(c). These motor modules contain brushless DC motors with multiple components integrated into one unit, as shown in Fig. 1(d).

Underwater manipulators are typically mounted on UUVs for operations, and installation space is usually limited. Thus, a foldable design is adopted for the manipulator, and this results in a significant reduction in the space it occupies when folded. The folding is achieved by employing a joint connector design with a 135° angle without compromising the operational radius, as shown in Fig. 2(a). Parts 3 and 5 in Fig. 1(b) are connectors. Conventional straight-linkage designs are unable to fold due to structural interference. The use of a 135°-angle design allows multiple links to be folded together, as shown in Fig. 2(d), resulting in a 30% reduction in overall height. Space is reserved for end-effector installation, which allows the manipulator to be folded even when end-effectors are attached. The folded dimensions are $488 \times 150 \times 280$ mm, occupying a space of approximately 0.02 m^3; This means it is easy to mount on a UUV, as Fig. 2(g) shows. The connector

TABLE II
WEIGHTS OF MAIN COMPONENTS.

Component	Weight in air (kg)	Weight in water (kg)
Structural Parts	4.196	1.698
Motor Modules	4.360	2.596
Other Parts	0.354	0.207
Total	8.910	4.501

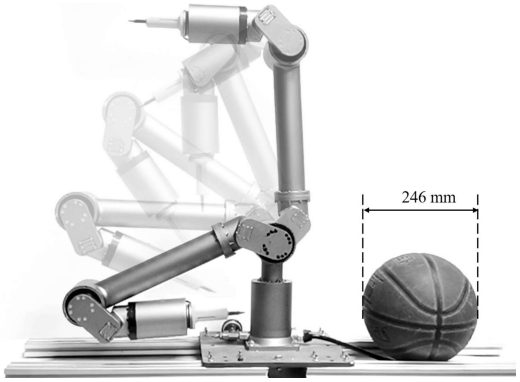

Fig. 3. Folding process of the manipulator prototype.

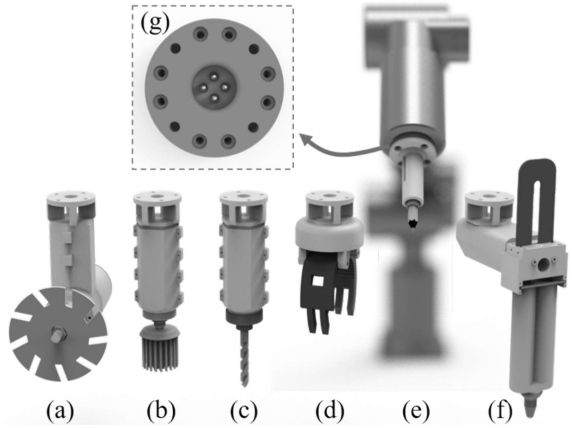

Fig. 4. Modular rapid-switching interface design for various end-effectors. (a) Underwater electric cutting tool. (b) Underwater electric brush. (c) Underwater electric drill. (d) Underwater electric gripper. (e) Underwater marking tool. (f) Underwater electric glue applicator. (g) Modular mechanical and electrical rapid-switching interfaces.

rods are hollow, so cables can be routed through them. This design offers the advantages of reducing external interference and facilitating installation, as shown in Figs. 2(b) and 2(e). The folding process of the prototype is shown in Fig. 3.

B. High Precision and High Payload

Electric underwater manipulators are powered by motors, and these often require a reducer to increase the torque. Commonly used reducers include planetary, harmonic, and cycloid reducers [23]. Harmonic reducers have high accuracy with zero backlash, and they have relatively small volume and weight. Therefore, a custom-made joint module with a harmonic reducer is applied in the manipulator described herein. Absolute encoders on the output of the drivetrain allow precise control of the velocity and position of the actuator, meeting the requirement for high precision from both the mechanical and electrical perspectives. The peak torque of the motor module can reach 143 Nm, which meets the 9-kg load capacity of the manipulator. The motor modules use bus communication, and only a single integral cable is needed to control all four motor modules, reducing the length and weight of cable required. In Fig. 1(e), the parts highlighted in red are waterproof connectors: the lower one is the control input interface, and the upper one is the output interface, which can be used for external end-effector control. After testing, it was found that the repeatability of the manipulator reached ± 0.01 mm, and its maximum payload is 9 kg.

C. Rapid-Switching Interface for End-Effectors

To achieve rapid switching between multiple end-effectors, the end of the manipulator is equipped with universal interfaces. Specifically, a universal flange interface is used for mechanical connections, as shown in Fig. 1(b)-7, while a four-core underwater electrical connector is used for the power-supply and control connections, as illustrated in Fig. 4(g). These interface designs facilitate the fast installation and control of various end-effectors. Six different underwater end-effectors are interchangeable for the manipulator, as depicted in Figs. 4(a)–4(f). Notably, when switching between end-effectors, only four fixed screws need to be installed, along with connection of the control interface, which can be completed on site during repair tasks without the need for factory replacements or rewiring. In actual tests, it was found that the tools can be switched within five minutes.

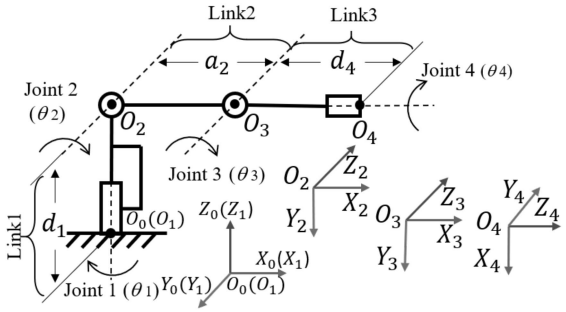

Fig. 5. D–H reference frames.

TABLE III
D–H PARAMETERS OF THE MANIPULATOR.

Link	θ (°)	d (mm)	a (mm)	α (°)
1	θ_1	223.5	0	90
2	θ_2	0	413.1	0
3	$\theta_3 + 90$	0	0	90
4	θ_4	218.5	0	0

D. Kinematics Analysis

The kinematics of the manipulator can be divided into forward and inverse kinematics. The initial position of the manipulator is defined in Fig. 5. Depending on the initial position, the Denavit–Hartenberg (D–H) reference frames including $O_0X_0Y_0Z_0$–$O_4X_4Y_4Z_4$ are assigned. All the joint angles are set to 0° when the manipulator is in the initial position. The D–H parameters of this manipulator are given in Table III. From this information, the solutions for the forward and inverse kinematics equations can be derived.

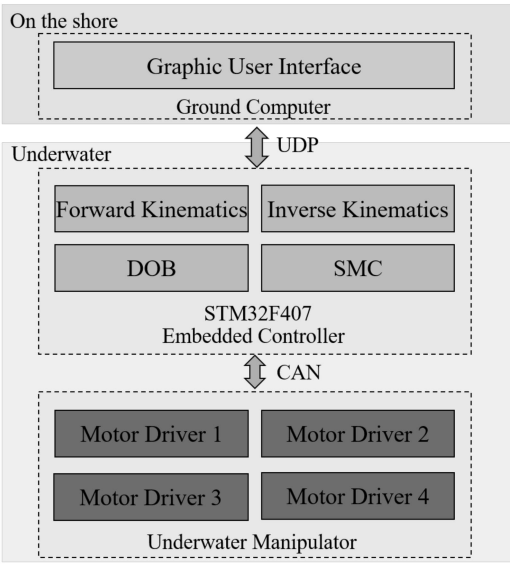

Fig. 6. Software architecture of the manipulator.

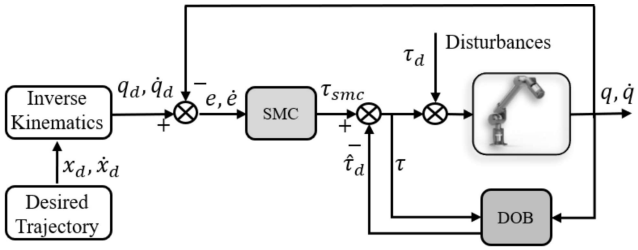

Fig. 7. Structure of the proposed robust controller.

III. Controller Design

A. Software Architecture

The control-software framework of the system is divided into two parts: onshore and underwater, as shown in Fig. 6. The onshore part is responsible for the user interface and communication with the underwater part through the user datagram protocol (UDP). The underwater part includes an underwater manipulator and an embedded controller. All four servo-motor modules of the underwater manipulator are connected to the embedded controller through a controller area network (CAN) bus. The maximum communication rate for both UDP and CAN is 200 Hz. The embedded controller is mainly used for calculating the forward and inverse kinematics and the DOB-SMC algorithm. Additionally, it controls the final direct torques, positions, and angles of the joint servo motors. An STM32F407 ARM-based microcontroller with a hardware floating-point arithmetic unit is used in the embedded controller, making it suitable for the motion control of the manipulator. In practice, the control board is capable of conducting the required calculations for four joints in just 0.47 ms, including the inverse and forward kinematics solution of the manipulator, and the control algorithm, which amply meets the real-time control demands of the manipulator.

B. Control Algorithm

The DOB-SMC robust controller algorithm was designed to ensure the control precision of the manipulator in fast-flowing water. The dynamic model of the underwater manipulator can be expressed as

$$\boldsymbol{M(q)\ddot{q} + C(q,\dot{q})\dot{q} + G(q) = \tau + \tau_d}, \tag{1}$$

where $\boldsymbol{M(q) \in R^{n\times n}}$ is the inertia matrix, $\boldsymbol{C(q,\dot{q}) \in R^{n\times n}}$ is the centrifugal and Coriolis matrix, $\boldsymbol{G(q) \in R^n}$ is the gravity matrix, q is the joint angle of the manipulator,$\boldsymbol{\tau \in R^n}$ is the control torque of the master manipulator, and $\boldsymbol{\tau_d \in R^n}$ is the external disturbance torque.

The joint trajectory-tracking error $\boldsymbol{e \in R^3}$ is defined as

$$\boldsymbol{e = q - q_d}, \tag{2}$$

where $\boldsymbol{q_d}$ is the desired joint angles calculated by inverse kinematics and the sliding surface is defined as

$$\boldsymbol{s = \dot{e} + ke}, \tag{3}$$

where $\boldsymbol{k} = \mathrm{diag}\,(k_1, k_2, k_3)$ $(k_i > 0)$. We then introduce a variable $\boldsymbol{q_r = \dot{q} - s}$, and obtain

$$\boldsymbol{\dot{q}_r = \dot{q} - ke, \ddot{q}_r = \ddot{q} - k\dot{e}}. \tag{4}$$

The SMC, which can keep the system asymptotically stable without a compensation controller, is designed as

$$\boldsymbol{\tau_{smc} = M(q)\ddot{q}_r + C(q,\dot{q})\dot{q}_r + G(q) - \beta\,\mathrm{sign}(s)}, \tag{5}$$

where β is the sliding gain that satisfies $\beta = \|\boldsymbol{\tau_d}\| + \delta$ $(\delta > 0)$ and $\boldsymbol{\tau_d}$ represents the disturbances.

The switching term in Eq. (5) may cause system chattering. Thus, a disturbance observer (DOB) was designed to estimate external disturbances and perform feed-forward compensation, which can eliminate chattering and enhance the system's robustness.

The DOB is represented as follows:

$$\begin{cases} \boldsymbol{\dot{z} = L(q)(C(q,\dot{q}) + G(q) - \tau) - L(q)\hat{\tau}_d}, \\ \boldsymbol{\hat{\tau}_d = z + p(\dot{q})}, \end{cases} \tag{6}$$

where: $\boldsymbol{\hat{\tau}_d}$, $\boldsymbol{z}$, and $\boldsymbol{p(\dot{q})}$ are the estimates of the disturbances, the internal state of the nonlinear observer, and the DOB auxiliary vector, respectively; $\boldsymbol{L(q)}$ is the DOB gain matrix that is to be designed. The DOB gain matrix and auxiliary vector can be designed as:

$$\boldsymbol{L(q) = X^{-1}M(q)^{-1}}, \tag{7}$$

$$\boldsymbol{p(\dot{q}) = X^{-1}\dot{q}}, \tag{8}$$

where $\boldsymbol{X \in R^{3\times 3}}$ is a reversible constant matrix, which can be adjusted in practical applications.

Therefore, the composite controller is designed as follows:

$$\boldsymbol{\tau = M(q)\ddot{q}_r + C(q,\dot{q})\dot{q}_r + G(q) - \delta\,\mathrm{sign}(s) - \hat{\tau}_d}, \tag{9}$$

where $\delta > 0$ is a small constant value that satisfies $\delta > \|\boldsymbol{\tau - \hat{\tau}_d}\|$.

A block diagram of the DOB-SMC is shown in Fig. 7. Since an appropriate manipulator was designed by the present authors, it was possible to obtain accurate dynamic parameters to verify the performance of the algorithm.

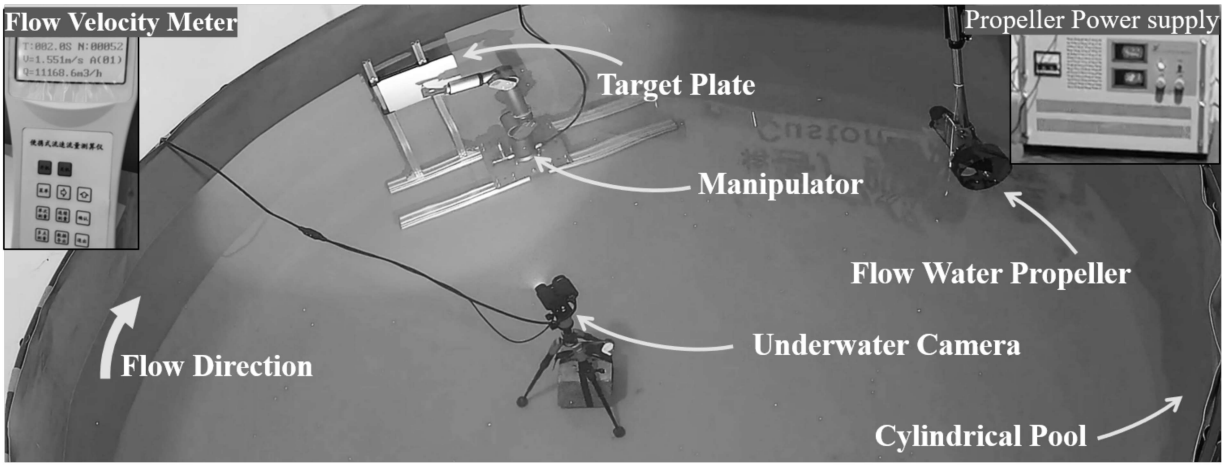

Fig. 8. Experimental setup of the flowing-water test.

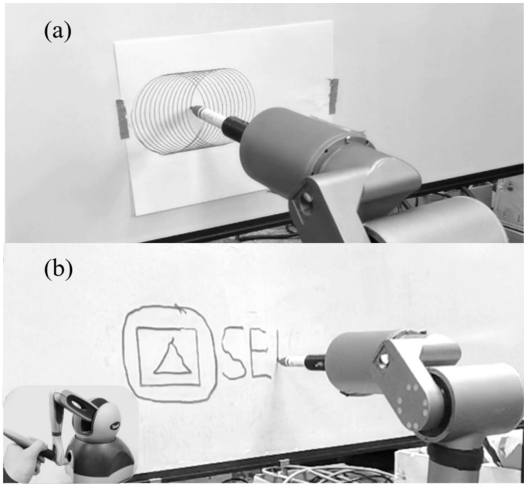

Fig. 9. Kinematics test with a marker tool. (a) Automatically drawing a spiral line using the embedded system. (b) Manual drawing of lines by a remote operator.

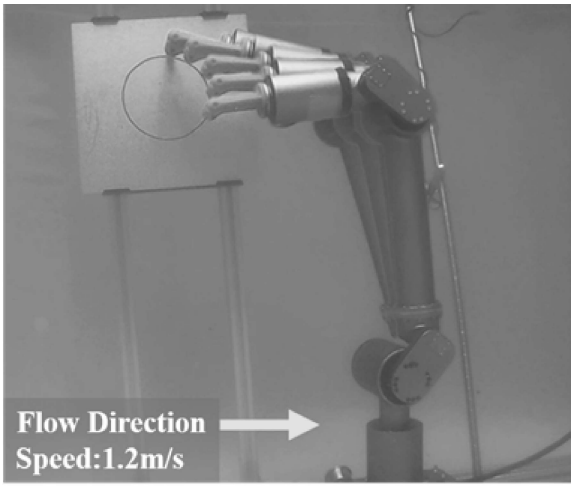

Fig. 10. Video frames of underwater marking task in flowing water.

IV. Experiments

A. Experimental Setup

To test the performance of the manipulator and the proposed algorithm in an underwater environment, we constructed a flowing-water test platform using a cylindrical canvas pool with a diameter of 3.0 m and a depth of 1.2 m. A 3.0-kW underwater propeller was used to generate a circulating water flow in this pool, reaching a maximum velocity of 1.5 m/s. We used a flow-velocity meter to measure the velocity of the water flow around the manipulator. An underwater camera was set to record the process of the whole test, as shown in Fig. 8. When compared to traditional circulating-water tanks that require construction of significant infrastructure, this platform is easy to assemble and disassemble and also cost-effective.

B. Algorithm Verification

Before we tested the manipulator under water, experiments were first conducted to examine its onshore kinematics. We migrated the kinematic models to the embedded system. Then, a marker tool was installed as the manipulator's end-effector, and a whiteboard was used as a target plate. The manipulator could thus be used to draw a trajectory on the whiteboard, which simulates the application of glue along a tiny crack. The automatic drawing of a spiral line and the manual drawing of shapes were tested, as shown in Fig. 9. The results show that the established kinematics model is correct, and it performs accurately under different operating conditions. Next, we conducted underwater tests.

Baseline marker/whiteboard tests without the DOB were initially conducted in flowing water at velocities of 0.0, 0.8, 1.0, and 1.2 m/s. Subsequently, tests with the DOB were performed for comparison purposes. As shown in the video frames in Fig. 10, the manipulator performed effectively in fast-flowing water.

Fig. 11 presents a comparison of trajectory-tracking performance. It can be seen that the accuracy of circular-trajectory tracking is significantly improved with the DOB enabled. This indicates that the proposed controller yields positive effects on

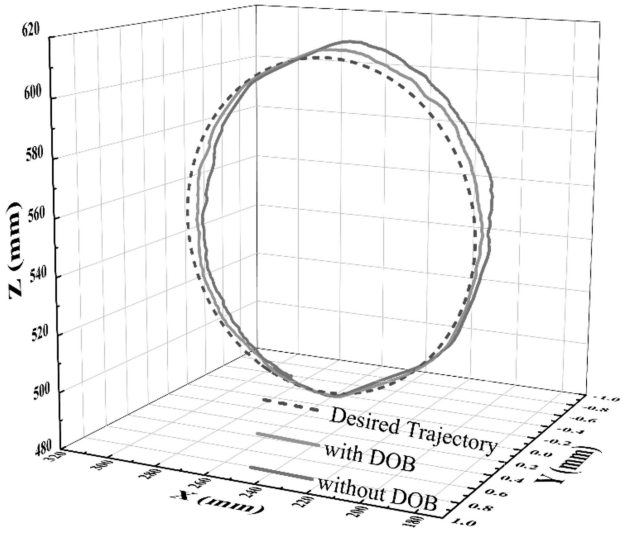

Fig. 11. Trajectories of marking operations with and without the DOB.

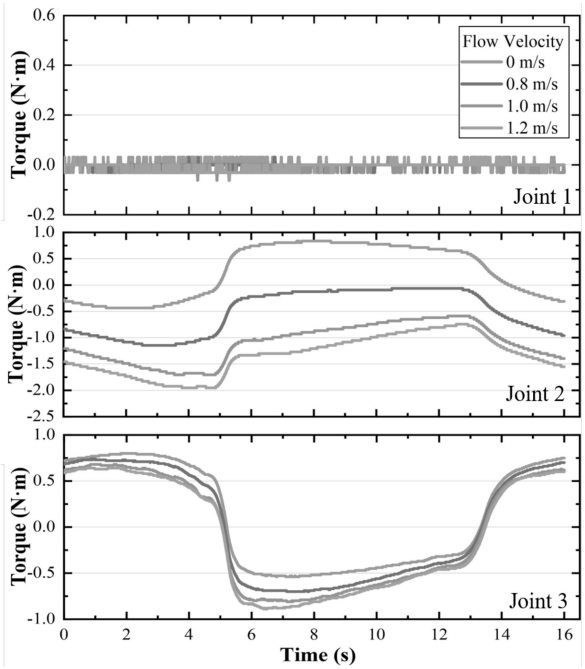

Fig. 12. Water-flow impact forces calculated by the DOB at different velocities.

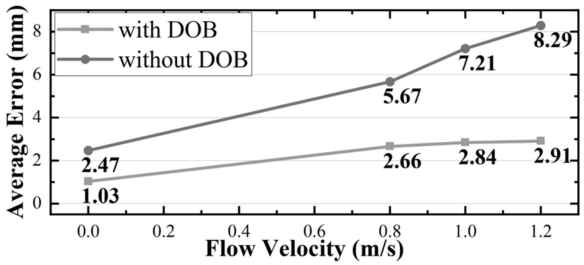

Fig. 13. Average trajectory errors of underwater marking operations at different water velocities.

tracking trajectories.

Fig. 12 displays the values of water-flow impact forces for each joint calculated by the DOB at four different flow velocities. The DOB calculates the external disturbance, which includes factors such as friction forces and water-flow disturbances. For this experiment, the main focus was on the water-flow disturbances. The core function of the proposed algorithm is the real-time calculation of external disturbance forces. The joints can then generate a reaction force of equal magnitude to counteract these external disturbance forces. Joint 1 maintains a fixed-point state with a desired angle of 0°, and the water-flow disturbance has minimal impact on the control torque. As a result, the DOB observation value for joint 1 is nearly zero, in line with the algorithm's expectation. In contrast, joints 2 and 3 are significantly affected by the water flow. Fig. 12 reveals that as the water-flow velocity was increased, the disturbance observation value also changed, exhibiting a positive-correlation trend. This finding verifies that the proposed algorithm is capable of accurately predicting and compensating for these disturbances.

Fig. 13 depicts trajectory-tracking error curves of the manipulator under various flow velocities. It is evident that the error is positively correlated with increasing flow rate, resulting in larger trajectory tracking errors. However, upon implementing DOB compensation, the errors are significantly reduced. For instance, at the maximum flow rate, with the DOB, the error decreases from 8.29 to 2.91 mm, a reduction of 5.38 mm. The use of the DOB enables effective control of the average trajectory error. Specifically, the minimum error was found to be 1.03 mm in still water and the maximum error was 2.91 mm in flowing water at 1.2 m/s. These improvements are evident in the results, demonstrating the effectiveness of the DOB in mitigating the trajectory-tracking errors of the manipulator under different flow velocities.

V. Conclusions

This paper presents the design and control of a novel lightweight underwater manipulator. To adapt to the needs of delicate underwater repair operations, we designed the manipulator to be lightweight and compact, making it easier to mount on UUVs. Motor modules with harmonic reducers are applied as the drivers, providing high precision and a high payload capacity. The end of the manipulator is designed with a rapid-switching interface for repair tools, which improves the efficiency of underwater repair operations. In terms of control, especially in complex underwater environments, a trajectory-tracking control strategy based on DOB-SMC is proposed. SMC, which is a robust nonlinear control strategy, is used as a feedback controller for the manipulator, and a DOB is used as a feed-forward compensation controller to estimate and compensate for underwater disturbances in real time. Actual underwater experiments demonstrated that the controller can significantly improve the trajectory-tracking accuracy of the manipulator in fast-flowing water, and this provides the necessary conditions for conducting delicate repair operations with

the manipulator. In the future, we will install the developed manipulator on an underwater robot and conduct tests in actual water-conservancy facilities such as tunnels and dams.

REFERENCES

[1] M. B. Skaldebø, B. O. Haugaløkken, and I. Schjølberg, "SeaArm-2 – fully electric underwater manipulator with integrated end-effector camera," in *Proc. IEEE Eur. Control Conf.*, 2021, pp. 236–242.

[2] S. Bartsch, A. Kolesnikov, C. Büskens, and M. Echim, "Modular underwater manipulators for autonomous underwater intervention," *AI Technol. Underwater Robot.*, vol. 96, pp. 95–103, 2020.

[3] M. Hildebrandt, J. Kerdels, J. Albiez, and F. Kirchner, "A multi-layered controller approach for high precision end-effector control of hydraulic underwater manipulator systems," in *Proc. IEEE OCEANS Conf.*, 2009, pp. 1–5.

[4] S. Sivčev, J. Coleman, E. Omerdić, G. Dooly, and D. Toal, "Underwater manipulators: A review," *Ocean Eng.*, vol. 163, pp. 431–450, 2018.

[5] C. Barbalata *et al.*, "Modelling and control of lightweight underwater vehicle-manipulator systems," Ph.D. dissertation, Heriot-Watt University, 2017.

[6] O. Forli, G. Raine, and R. Whillock, *Non-Destructive Examination of Underwater Welded Structures*. Woodhead Publishing, 1999, vol. 1372.

[7] B. Fletcher, "Worldwide undersea MCM vehicle technologies," Space and Naval Warfare System Center, San Diego, CA, Tech. Rep., 2000.

[8] S. Sivčev, M. Rossi, J. Coleman, G. Dooly, E. Omerdić, and D. Toal, "Fully automatic visual servoing control for work-class marine intervention ROVs," *Control Eng. Prac.*, vol. 74, pp. 153–167, 2018.

[9] C. C. Chang, C. Y. Chang, and Y. T. Cheng, "Distance measurement technology development at remotely teleoperated robotic manipulator system for underwater constructions," in *Proc. Int. Symp. Underwater Technol.*, 2004, pp. 333–338.

[10] S. Noé, T. Beck, A. Foubert, and A. Grehan, "Surface samples in Belgica Mound Province, Hovland Mound Province, West Rockall Bank, and Northern Porcupine Bank," Universität Bremen In: Ratmeyer, V., Hebbeln, D. & Shipboard Party: Report and Preliminary Results of RV Meteor Cruise M61/3, Tech. Rep., 2006.

[11] D. O. Jones, "Using existing industrial remotely operated vehicles for deep-sea science," *Zool. Scr.*, vol. 38, pp. 41–47, 2009.

[12] R. D. Christ and R. L. Wernli Sr, *The ROV Manual: A User Guide for Remotely Operated Vehicles*. Butterworth-Heinemann, 2013.

[13] Y. Wang, M. Cai, S. Wang, X. Bai, R. Wang, and M. Tan, "Development and control of an underwater vehicle–manipulator system propelled by flexible flippers for grasping marine organisms," *IEEE Trans. Ind. Electron.*, vol. 69, no. 4, pp. 3898–3908, 2021.

[14] Y. Wang, S. Wang, Q. Wei, M. Tan, C. Zhou, and J. Yu, "Development of an underwater manipulator and its free-floating autonomous operation," *IEEE/ASME Trans. Mechatronics*, vol. 21, no. 2, pp. 815–824, 2015.

[15] Z. Shen, H. Zhong, E. Xu, R. Zhang, K. C. Yip, L. L. Chan, L. L. Chan, J. Pan, W. Wang, and Z. Wang, "An underwater robotic manipulator with soft bladders and compact depth-independent actuation," *Soft Robot.*, vol. 7, no. 5, pp. 535–549, 2020.

[16] Z. Gong, X. Fang, X. Chen, J. Cheng, Z. Xie, J. Liu, B. Chen, H. Yang, S. Kong, Y. Hao, *et al.*, "A soft manipulator for efficient delicate grasping in shallow water: Modeling, control, and real-world experiments," *Int. J. Robot. Res.*, vol. 40, no. 1, pp. 449–469, 2021.

[17] J. Koch, T. Pailevanian, M. Garrett, C. Yahnker, R. Detry, D. Levine, and M. Gildner, "Development of a robotic limb for underwater mobile manipulation," in *Proc. IEEE Kobe TechnoOceans (OTO)*, 2018, pp. 1–5.

[18] G. Antonelli *et al.*, *Underwater Robots: Motion and Force Control of Vehicle-Manipulator Systems*. Springer, 2006, vol. 2.

[19] J. Smith, R. Yu, I. Sarafis, and J. Lucas, "Computer vision control of an underwater manipulator," in *Proc. OCEANS' 94*, vol. 1, 1994, pp. I–187.

[20] É. L. Oliveira, R. M. Orsino, and D. C. Donha, "Disturbance-observer-based model predictive control of underwater vehicle manipulator systems," *IFAC-PapersOnLine*, vol. 54, no. 16, pp. 348–355, 2021.

[21] M. Lee and H.-S. Choi, "A robust neural controller for underwater robot manipulators," *IEEE Trans. Neural Netw.*, vol. 11, no. 6, pp. 1465–1470, 2000.

[22] J. Li, P. Liu, S. Wang, and J. Leng, "Finite element analysis of O-ring sealing performance of manned submersible viewports," *J. Failure Anal. Prevent.*, vol. 20, pp. 1628–1637, 2020.

[23] A.-D. Pham and H.-J. Ahn, "High precision reducers for industrial robots driving 4th industrial revolution: State of arts, analysis, design, performance evaluation and perspective," *Int. J. Precis. Eng. Manuf. - Green Technol.*, vol. 5, pp. 519–533, 2018.